Sigma J Eng Nat Sci, Vol. 44, No. 3, pp. 2183−2194, June, 2026

Sigma Journal of Engineering and Natural Sciences
Web page info: https://sigma.yildiz.edu.tr
DOI: 10.14744/sigma.2026.2088

Research Article

Magnetic field effects on fluid flow and heat transfer in silver nanoparticle-water nanofluid: A numerical analysis

Farooq SHAIK[1,*]

[1]*Department of Mechanical Engineering, Vignan's Foundation for Science Technology and Research, Vadlamudi, Andhra Pradesh, 522213, India*

ARTICLE INFO

Article history
Received: 05 November 2024
Revised: 30 December 2024
Accepted: 06 April 2025

Keywords:
Magnetic Field; Nanoparticles Volume Fraction; Natural Convection; Nusselt Number; Rayleigh Number

ABSTRACT

This study numerically investigates the effect of a magnetic field on the natural convective heat transfer of silver nanoparticle-water nanofluid within a square cavity. The cavity is heated from below, with its vertical side walls kept at a constant lower temperature, while the top surface is adiabatic and a constant magnetic field is applied to the left vertical surface. The effects of Rayleigh number (10^3 to 10^6), Hartmann number (0 to 20), and nanoparticle volume fraction (2% to 8%) on heat transfer and fluid flow characteristics are analyzed. The results show that increasing the nanoparticle concentration significantly increases the heat transfer in the enclosure at higher values of Rayleigh number. Contrary, increasing Hartmann number, reduces the fluid velocities and average Nusselt number due to the effect of Lorentz forces. This dual influence highlights the potential for optimized thermal management in diverse applications. The novelty of this work lies in investigating the silver-water nanofluids under varying magnetic field and buoyancy forces in enclosed geometries offering new insights into engineering applications.

Cite this article as: Shaik F. Magnetic field effects on fluid flow and heat transfer in silver nanoparticle-water nanofluid: A numerical analysis. Sigma J Eng Nat Sci 2026;44(3):2183−2194.

INTRODUCTION

Natural convection heat transfer plays a crucial role across numerous utilizations, involving energy storage devices, nuclear reactor cooling, and microelectronic component thermal management. Optimizing this process within closed cavities hinges on the characteristics of the enclosed fluid. Traditional heat transfer fluids often present limitations, making heat transfer enhancement a crucial area of research [1]. Nanofluids (NFs), engineered suspensions of nanoparticles within a base fluid, offer a promising solution. Studies by Choi et al. [2] demonstrated that nanoparticles enhance the thermal conductivity of fluids like water. Commonly used nanoparticles include silver, copper oxide, and aluminum oxide have higher thermal conductivity [3-5]. Magnetic field effect on NFs is crucial in engineering due to its capabilities in altering fluid circulations, flow patterns and temperature distribution [6-8]. The applied magnetic field causes a Lorentz force that relates with the buoyancy force within the fluid [9]. By tactically altering this interaction, researchers can potentially alter

***Corresponding author.**
*E-mail address: farooq.314@gmail.com

This paper was recommended for publication in revised form by Editor-in-Chief Ahmet Selim Dalkilic

Published by Yıldız Technical University Press, İstanbul, Turkey

fluid velocities and effects heat transfer patterns [10, 11]. Saha et al. [12] numerically analyzes MHD-driven heat transfer and reported that blade-shaped nanoparticles enhance heat transfer, outperforming spherical ones. Rahman et al. [13] reported that increasing the micro-rotation and Hartmann number reduces Nu_{avg} and natural convection. The Bejan number increases as Rayleigh number decreases, and Nuavg drops by 24% with the inclination angle change from 0° to 90°. Javed and Siddiqui [14] performed simulations to analyze how a magnetic field affects heat transfer in a ferrofluid (magnetic liquid) inside a square cavity. They found that strength of magnetic field significantly affect how heat flows within the cavity. Balla et al. [15] studied heat transfer in a tilted cavity with liquid containing nanoparticles and saturated with a porous material. The simulations consider different nanoparticle types (copper, aluminum oxide, etc.) and a magnetic field. They analyze how these factors, along with the temperature difference and cavity angle, influence heat transfer. Selimefendigil and Oztop [16] examines water-based NFs (Cu, Al_2O_3, TiO_2) and shows the heat transfer of 4%. Cylinder rotation impacts the Nusselt number, with a maximum 8.5% difference between Cu and Al_2O_3. At the highest volume fraction, Cu-water NF enhances heat transfer by 38.10%. A polynomial correlation for the Nusselt number was developed, dependent on Rayleigh number and cylinder rotation speed. Sheikholeslami et al. [17] reported heat transfer rate decreases with increasing Ha. Rahman et al. [18] numerically investigates alumina-water NF using Buongiorno's mathematical model. They concluded that magnetic field have strong influence on fluid circulation patterns and temperature distribution. Sreedevi and Reddy [19] reported that a stronger magnetic field led to an increase in the temperature of the NF inside the cavity. Acharya et al. [20] simulates heat transfer of alumina-water NF. The bottom and top are partly heated, with three parallel fins (cooled on sides, heated in middle) inside. Uddin et al. [21] investigates copper oxide-water NF inside a enclosure with a wavy bottom wall. Results show that NF has lower friction than the base fluid, and friction increases with higher RaN and nanoparticle diameter. Dutta et al. [22] investigates Cu-water NFs inside rhombic cavities. It was reported that total entropy production reduces with increasing Ha. Alhajaj et al. [23] compared heat extraction using different NFs and configurations. The best overall performer was 0.5% alumina in water. Fayz-Al-Asad et al. [24] explored MHD based heat transfer employing a finite element method. The study shows that the heat transfer improves with stronger buoyancy force but reduces with a stronger magnetic field. Alqaed et al. [25] studied alumina-water NFs in a cavity with inclined walls using a numerical technique. They found that a higher cavity angle improved heat transfer and the cavity angle was 30 degrees. Song et al. [26] explored the flow of a ferromagnetic NF in a channel that has dimples and a heated blockade. Their results showed that stronger flow rates significantly improve heat transfer at the dimpled surface. Thermal management is a crucial task through varied engineering applications, relating to renewable energy, automotive technologies, and cryogenic storage. Literature has highlighted the importance of enhanced materials and advanced heat transfer solutions to direct these tasks [27-30]. Although findings on NFs under magnetic fields have managed advancement, there is inadequate emphasis on Ag based NFs although their advanced thermal properties. Ag nanoparticles demonstrate various benefits related to normally employed nanoparticles, such as alumina or copper oxide [31-34]. However, the high cost of silver nanoparticles remains a significant challenge, influenced by factors such as raw material prices, synthesis methods (e.g., chemical reduction, laser ablation, and green synthesis), production scale, and purity requirements for specific applications [35-37]. The objective of the work is to investigate the effects of nanoparticle, buoyancy forces, and magnetic field on NF within a square cavity.

PROBLEM FORMULATION

A schematic illustration of a square cavity is shown in Figure 1a. The lower horizontal surface has a heat source with a constant temperature, T_h, the upper surface is adiabatic and the vertical surfaces are kept at a cold temperature, T_c. A constant horizontal magnetic field is applied to

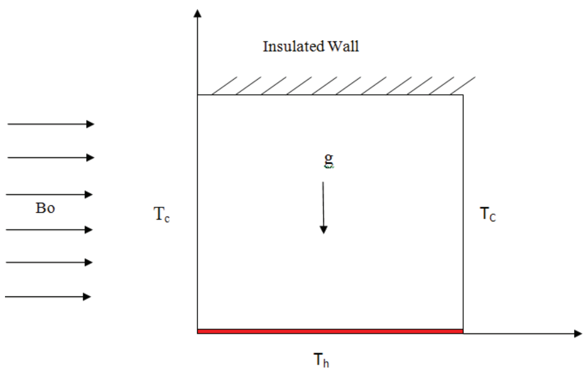

Figure 1a. Schematic view of the problem.

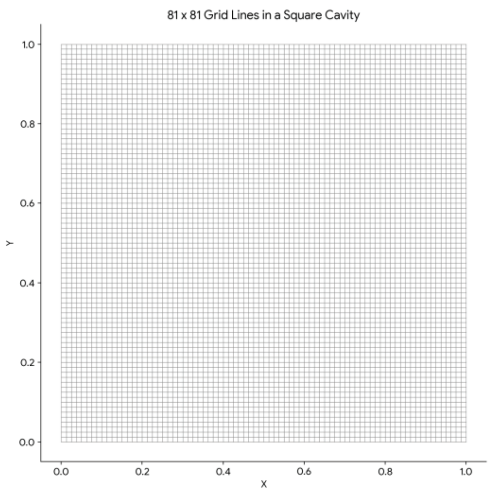

Figure 1b. Grid lines.

the left vertical surface. The parameters are taken to be constant and the density change of NFs is taken into account using the Boussinesq equation. Figure 1b illustrates the computational domain along with the grid lines.

Governing Equations

The following are the governing equations used in the present study [38, 39]:

$$\frac{\partial \bar{u}}{\partial x}+\frac{\partial \bar{v}}{\partial y}=0 \quad (1)$$

$$\bar{u}\frac{\partial \bar{u}}{\partial x}+\bar{v}\frac{\partial \bar{u}}{\partial y}=\frac{1}{\rho_{n\_f}}\left[-\frac{\partial \bar{p}}{\partial x}+\mu_{n\_f}\left(\frac{\partial^2 \bar{u}}{\partial x^2}+\frac{\partial^2 \bar{u}}{\partial y^2}\right)\right] \quad (2)$$

$$\bar{u}\frac{\partial \bar{v}}{\partial x}+\bar{v}\frac{\partial(\bar{v})}{\partial y}=\frac{1}{\rho_{n\_f}}\left[-\frac{\partial \bar{p}}{\partial y}+\mu_{n\_f}\left(\frac{\partial^2 \bar{v}}{\partial x^2}+\frac{\partial^2 \bar{v}}{\partial y^2}\right)+(\rho\beta)_{n\_f}g(\bar{T}-\bar{T}_c)-\sigma_{n\_f}B_0^2\bar{v}\right] \quad (3)$$

$$\bar{u}\frac{\partial T}{\partial x}+\bar{v}\frac{\partial T}{\partial y}=\alpha_{n\_f}\left[\left(\frac{\partial^2 T}{\partial x^2}+\frac{\partial^2 T}{\partial y^2}\right)\right] \quad (4)$$

The thermo-physical properties of nano fluids are determined by [40, 41]:

$$\rho'_{n\_f}=(1-\chi)\rho'_f+\chi\rho'_s \quad (5)$$

$$\alpha_{n\_f}=k_{n\_f}/(\rho' C_p)_{n\_f} \quad (6)$$

$$(\rho' C_p)_{n\_f}=(1-\chi)(\rho' C_p)_f+\chi(\rho' C_p)_s \quad (7)$$

$$(\rho'\beta)_{n\_f}=(1-\chi)(\rho'\beta)_f+\chi(\rho'\beta)_s \quad (8)$$

$$\mu_{n\_f}=\frac{\mu_f}{(1-\chi)^{2.5}} \quad (9)$$

$$k_{n\_f}=k_f\left[\frac{(k_s+2k_f)-2\chi(k_f-k_s)}{(k_s+2k_f)+\chi(k_f-k_s)}\right] \quad (10)$$

$$\sigma_{n\_f}=(1-\chi)\sigma_f+\chi\sigma_s \quad (11)$$

Dimensionless terms are uses are:

$$X'=x/L,\ Y'=y/L,\ \bar{U}=\frac{\bar{u}L}{\alpha_f},\ \bar{V}=\frac{\bar{v}L}{\alpha_f},\ \bar{P}=\frac{\bar{p}L^2}{\rho_{nf}\alpha_f^2},\ \theta=\frac{(\bar{T}-\bar{T}_c)}{(\bar{T}_h-\bar{T}_c)}. \quad (12)$$

$$\frac{\partial U}{\partial X'}+\frac{\partial V}{\partial Y'}=0 \quad (13)$$

$$\bar{U}\frac{\partial \bar{U}}{\partial X'}+\bar{V}\frac{\partial \bar{U}}{\partial Y'}=-\frac{\partial \bar{P}}{\partial X'}+\frac{\mu_{nf}}{\rho_{nf}\alpha_f}\left(\frac{\partial^2 \bar{U}}{\partial X'^2}+\frac{\partial^2 \bar{U}}{\partial Y'^2}\right) \quad (14)$$

$$\bar{U}\frac{\partial \bar{V}}{\partial X'}+\bar{V}\frac{\partial \bar{V}}{\partial Y'}=-\frac{\partial \bar{P}}{\partial Y'}+\frac{\mu_{nf}}{\rho_{nf}\alpha_f}\left(\frac{\partial^2 \bar{V}}{\partial X'^2}+\frac{\partial^2 \bar{V}}{\partial Y'^2}\right)+\frac{(\rho\beta)_{nf}}{\rho_{nf}\beta_{nf}}RaN\,Pr\,\bar{\theta}-Ha^2\,Pr\,\bar{V} \quad (15)$$

$$\bar{U}\frac{\partial \bar{\theta}}{\partial X'}+V\frac{\partial \bar{\theta}}{\partial Y'}=\frac{\alpha_{n\_f}}{\alpha_f}\left[\left(\frac{\partial^2 \bar{\theta}}{\partial X'^2}+\frac{\partial^2 \bar{\theta}}{\partial Y'^2}\right)\right] \quad (16)$$

$$RaN=\frac{g\beta_f L^3((\bar{T}_h-\bar{T}_c))}{\nu_f\alpha_f} \quad (17)$$

$$Pr=\frac{\nu_f}{\alpha_f} \quad (18)$$

$$Ha^2=\frac{\sigma_{n\_f}B_0^2L^2}{\mu} \quad (19)$$

The Nusselt number (local and average) along the heated surface is determined by:

$$Nu_l=-\frac{k_{n\_f}}{k_f}\frac{\partial \bar{\theta}}{\partial Y}\bigg|_{Y=0} \quad (20)$$

$$Nu_{avg}=\frac{1}{A}\int_0^1 Nu_l\,dA \quad (21)$$

Boundary Conditions

Table 1 shows the applied velocity and thermal boundary conditions to the enclosure

Table 1. Boundary conditions

Boundary	Thermal Condition	Velocity Condition
Left boundary	Cold (θ=0)	No slip condition
Right boundary	Cold (θ=0)	
Top boundary	Adiabatic ($\frac{\partial\theta}{\partial Y}=0$)	
Bottom boundary	Hot (θ=1)	

Table 2. Thermo-physical properties (Data compiled from [42])

	Density (kg/m³)	Specific heat (J/kg K)	Thermal conductivity (W/m K)	Thermal expansion coefficient (1/K)
Water	997.1	4179	0.63	21×10^{-5}
Ag	10500	235	429	1.89×10^{-5}

Numerical Solution and Code Validation

The steady state governing equations were solved using the finite volume method. The Semi-Implicit Method for Pressure-Linked Equations algorithm was applied for pressure-velocity coupling. The resulting discretized equations was handled with the Tri-Diagonal Matrix Algorithm. [43]. The computational code, developed in C++, was designed with a convergence criterion of 10^{-6} for all variables. To validate its accuracy, the code was benchmarked against results reported by Ghasemi et al. [44]. The validation process involved simulating the enclosure using an Al_2O_3-water NF, taking into account its boundary conditions and fluid properties. The computed results were compared Ghasemi et al.'s findings in terms of the Nu_{avg} and flow streamlines at given RaN and Ha. The simulation results from the developed code exhibited excellent agreement with those stated by Ghasemi et al. [44], as shown in Table 3 and Figure 2.

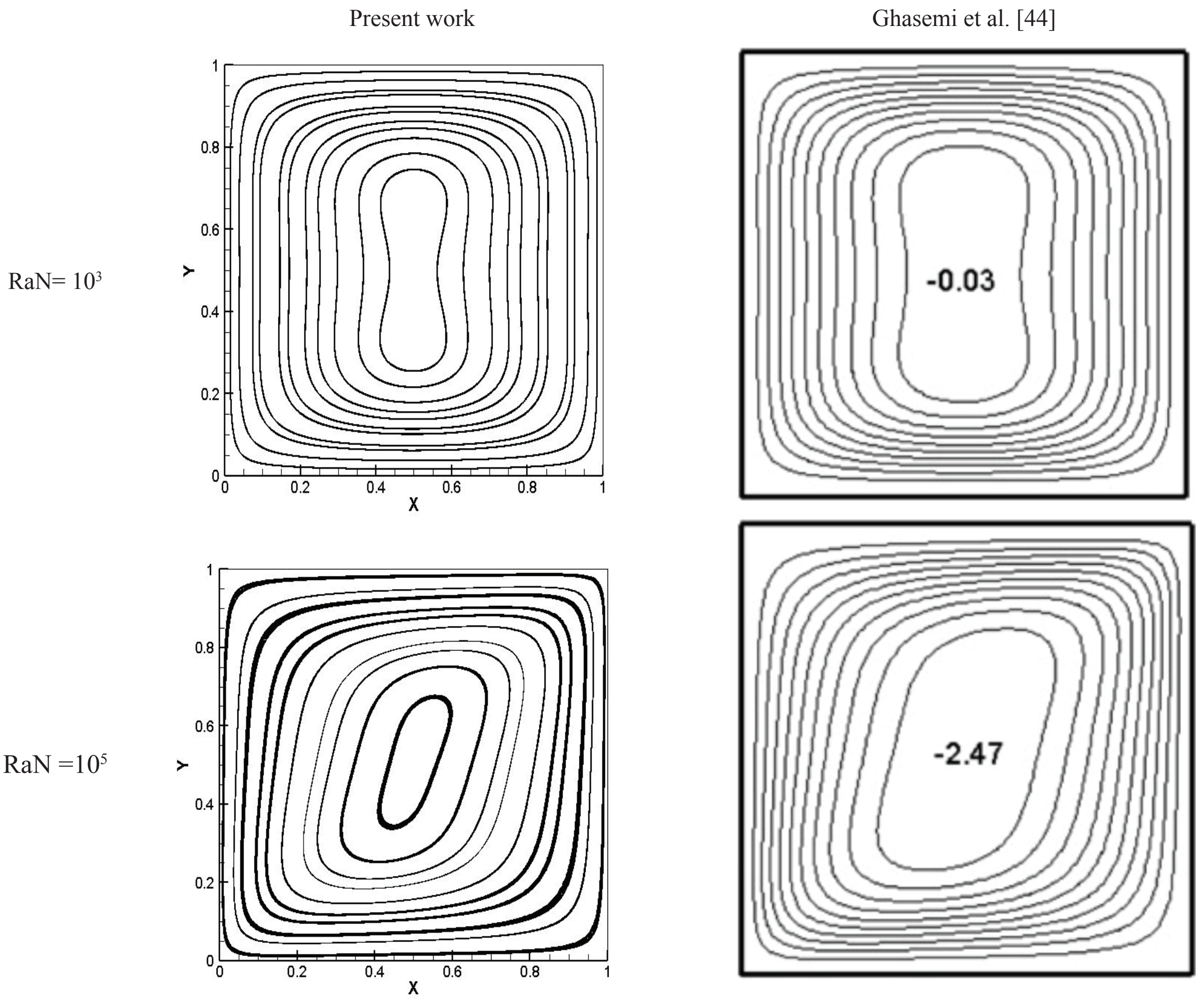

Figure 2. Similarity of streamlines with results of Ghasemi et al. [44] (RaN= 10^3 and 10^5, Ha=60).

Table 3. Validation of Nu_{avg} with Ghasemi et al. [44] at Ha=30 [Data adapted from Ghasemi et al. [44] for validation purposes]

	Present Work		**Ghasemi et al. [44]**	
	χ=4%	**χ=6%**	**χ=4%**	**χ=6%**
RaN = 10^3	1.116	1.173	1.121	1.184
RaN= 10^4	1.191	1.237	1.249	1.291
RaN = 10^5	3.097	3.126	3.124	3.108
RaN = 10^6	8.036	8.064	8.042	8.098

Grid Sensitivity Analysis

The study considers a square cavity of unit dimensions (1x1). This analysis was performed for a nanoparticle volume fraction of 4%. Table 4 shows the Nu_{avg} exhibited negligible variation between 81x81 and 121x121 grid configurations at a RaN of 10^4. Consequently, an 81x81 grid was adopted for subsequent analyses balancing computational efficiency and solution accuracy.

RESULTS AND DISCUSSION

This study primarily investigates how magnetic field, buoyancy forces and φ influences the flow patterns, fluid velocities, temperature distribution, and convective heat transfer. The selected range of RaN encompasses scenarios from weak to strong convection, covering a broad spectrum of natural convection phenomena. The Ha, ranging from 0 to 20, is selected to study the scenarios where magnetic forces transition from negligible to dominant, showcasing their suppressive effect on convective currents. A constant Pr value of 7 was chosen in the present study [45].

Impact of RaN on Streamlines

Figure 3 illustrates the formation of streamline patterns within the cavity for varying RaN. At low RaN (10^3 and 10^4), viscous forces predominate, resulting in low fluid motion

Table 4. Grid sensitivity test (χ =4%, RaN=10^4, Ha=10, Pr = 7.0)

Grid	21x21	41x41	61x61	81x81	101x101	121x121
Nuavg	12.78	13.74	13.97	14.3	14.344	14.457

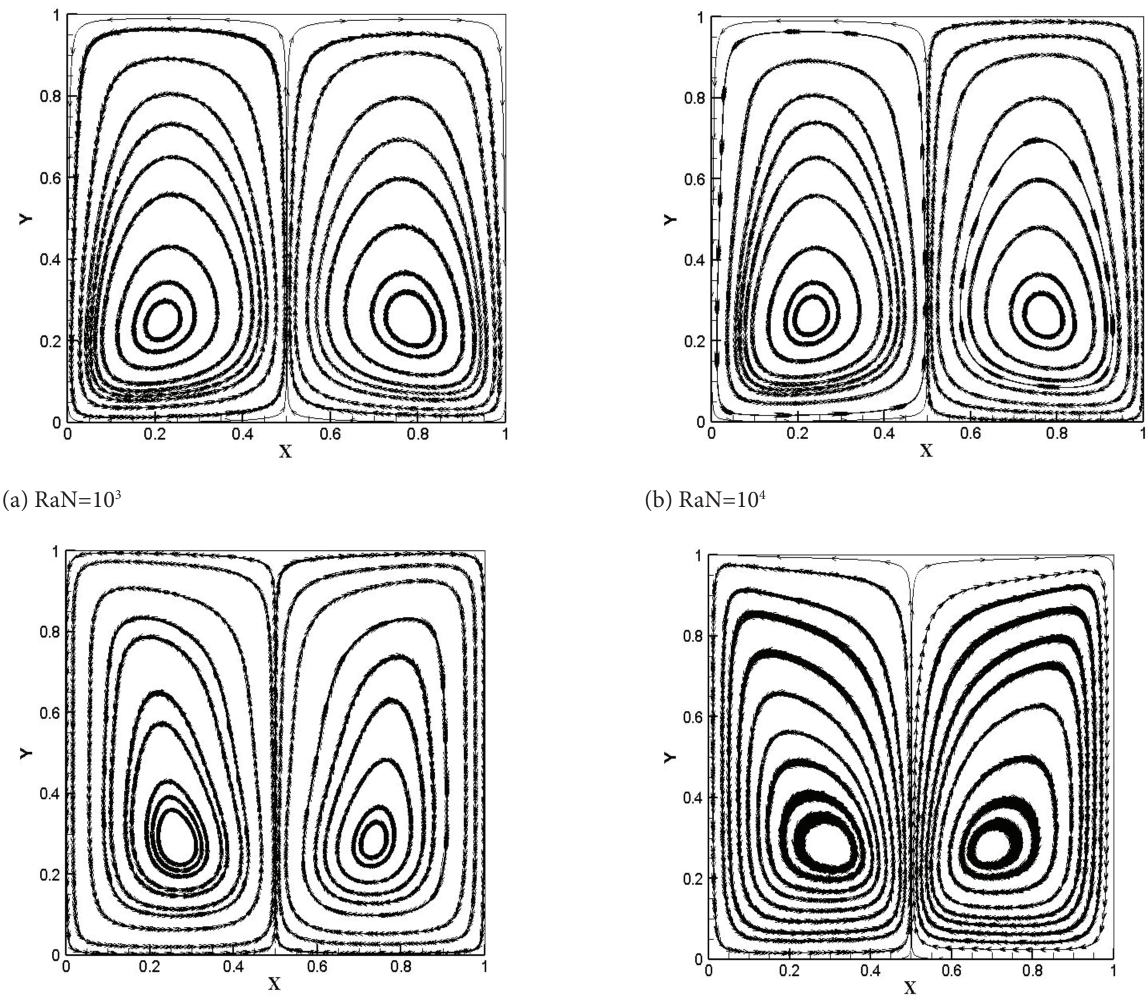

(a) RaN=10^3 (b) RaN=10^4 (c) RaN=10^5 (d) RaN=10^6

Figure 3. Stream lines for different RaN for χ =4% and Ha=20.

within the cavity. This indicates to a weak buoyant force exerted on the fluid. With an increase in the RaN, (10^5 and 10^6), the temperature difference becomes more significant, leading to a stronger buoyancy force. These loops represent the movement of the fluid as it rises due to buoyancy, cools down at the top, and descends along the colder walls [45]. The results demonstrates that for all nanoparticle volume fractions (χ = 2%, 4%, 6%, and 8%), increasing the RaN from 10^3 to 10^6 enhances fluid motion and convective heat transfer. While the trends are generally consistent across all φ values, the magnitude of enhancement in Nu_{avg} is higher for larger nanoparticle concentrations, owing to the increased thermal conductivity.

Impact of Ha on Streamlines

It is observed in Figures 4a-e that the opposite circulating fluid vortices, above the heat source, rises with raise in Ha. In the absence of Ha, the heated NF near the bottom

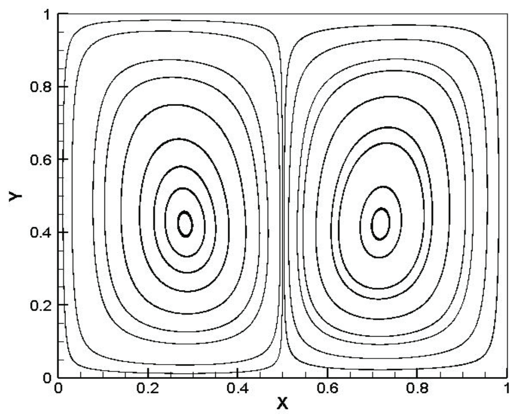

(a) Ha=0

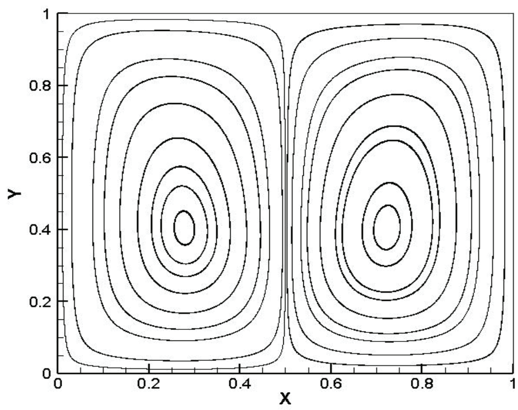

(b) Ha=5

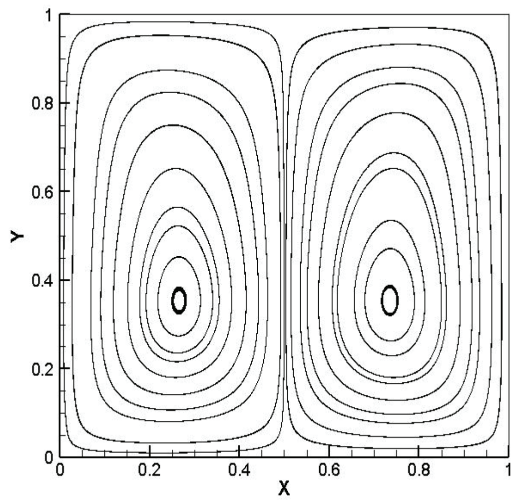

(c) Ha=10

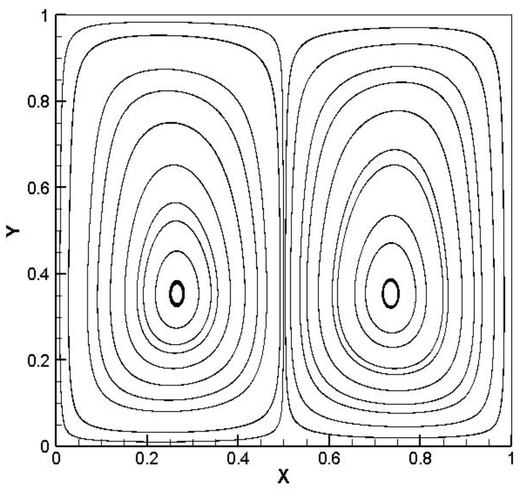

(d) Ha=15

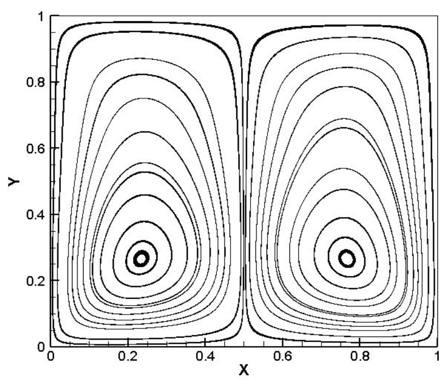

(e) Ha=20

Figure 4. Stream lines for different Ha for χ =2% and RaN=10^4.

surface experiences buoyancy forces that cause it to rise. This rising fluid creates a circulation pattern within the cavity. The cooler fluid from the top descends to replace the rising hot fluid, forming multiple smaller loops depending on the dominance of buoyancy forces. These circulation patterns are visualized by streamlines. When a magnetic field is introduced, the Lorentz effect acts against NF circulations. These forces weaken the circulation patterns within the cavity. The streamlines become less defined, with the loops becoming smaller and weaker. At high Ha, the convection currents can be almost entirely suppressed.

Impact of Ha on Isothermal Lines

Figure 5a-e illustrates that in the absence of Ha, the heated NF near the bottom surface rises due to buoyancy.

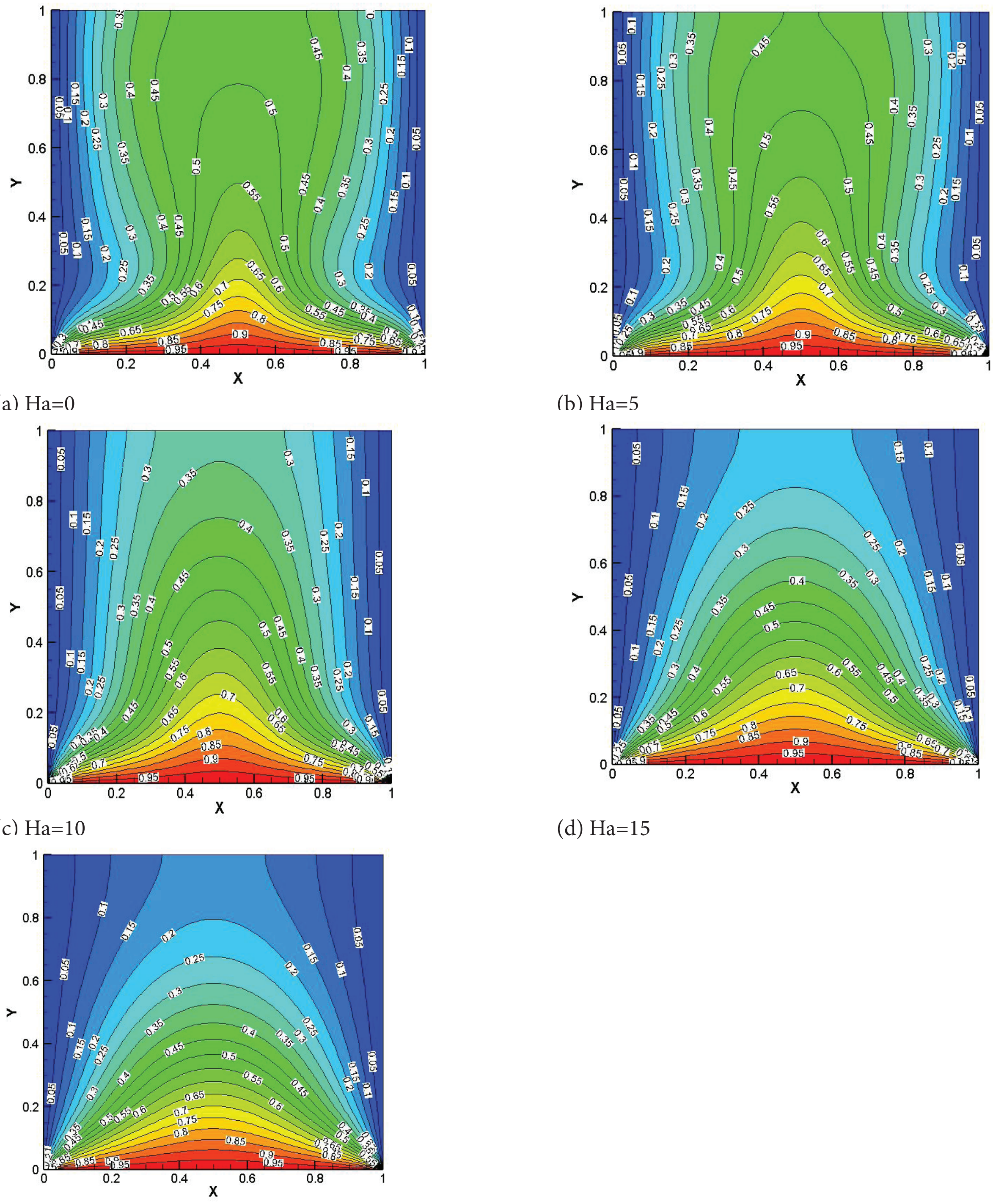

(a) Ha=0 (b) Ha=5 (c) Ha=10 (d) Ha=15 (e) Ha=20

Figure 5. Visualization of isothermal lines within a square cavity for different Ha at χ of 2% and RaN of 10^4.

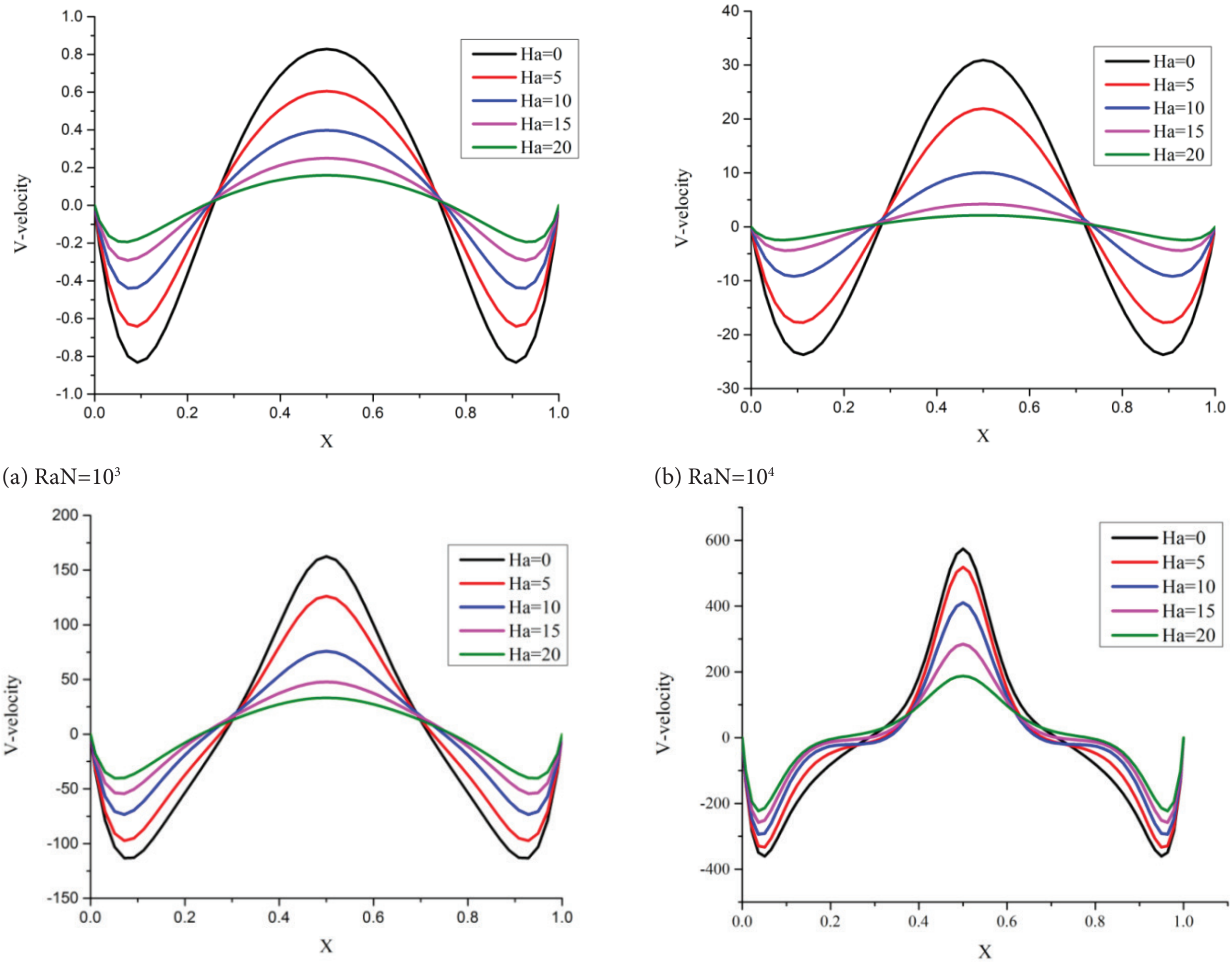

(a) RaN=10^3 (b) RaN=10^4

(c) RaN=10^5 (d) RaN=10^6

Figure 6. Influence of Ha on the mid-horizontal V-velocity at an χ =2%.

This creates circulation patterns that transport heat throughout the cavity. The isotherms, therefore, become spaced out, indicating a gradual temperature change across the cavity. When a Ha is introduced, the Lorentz effect hinders this movement. The isotherms become nearly parallel to the hot bottom surface, signifying a minimal temperature change along the vertical direction. In essence, a stronger magnetic field leads to thicker thermal layers near the heat source [46].

Impact of Magnetic Field on the Vertical Velocity Component (V) Along the Central Horizontal Axis of the Square Cavity

Figure 6a-d shows that the NF motion within the cavity is controlled by a balance involving buoyancy and viscous forces. The magnetic field introduces an additional retarding effect that dampens the fluid circulations. This effect opposes the circulation of the fluid, effectively acting like a drag. As Ha increases, the influence impedes the vertical circulation of the NF. The application of a Ha disrupts the fluid circulations induced by the temperature differential between the heated bottom and cooled top surfaces.

Impact of Ha on NUavg ALONG the Bottom Surface

Figure 7a-e shows that as χ increases, the effective thermal conductivity of the NF also improves compared to the base fluid. At lower Rayleigh numbers (RaN=10^3 and 10^4), heat transfer is mainly presided by conduction, resulting in only a slight increase in Nu_{avg}. However, as RaN increases to $10^5$and 10^6, along with a higher χ, convective heat transfer happen to major than conduction. As χ rises from 2% to 8%, Nu_{avg} experiences a notable 25% improvement, showcasing the superior heat conduction characteristics of the Ag-water NF. Conversely, increasing the Ha for a fixed RaN, the flow velocity reduces, inhibiting natural convection and leading to a lower Nu_{avg} by 40% at Ha= 20, similar effects were reported in the literature [47].

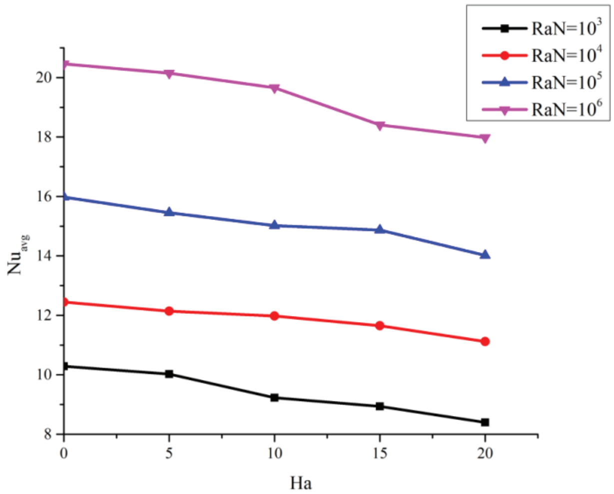

(a) $\chi = 0\%$

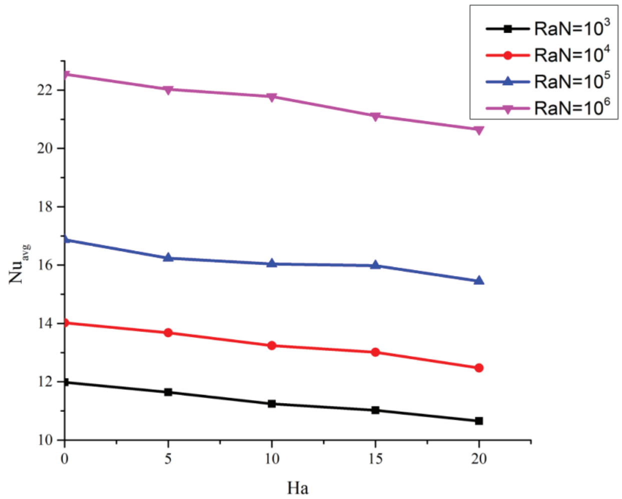

(b) $\chi = 2\%$

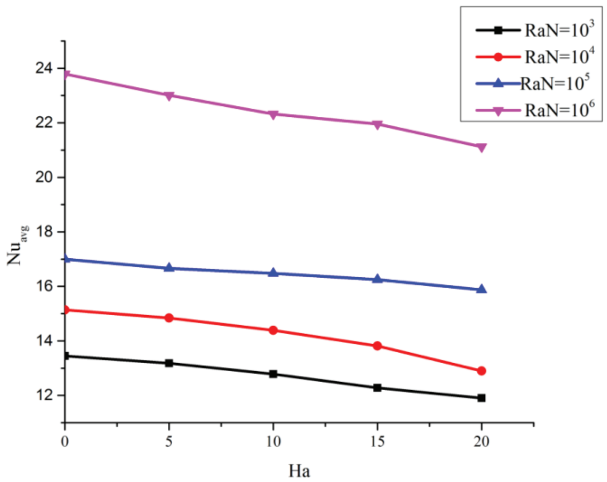

(c) $\chi = 4\%$

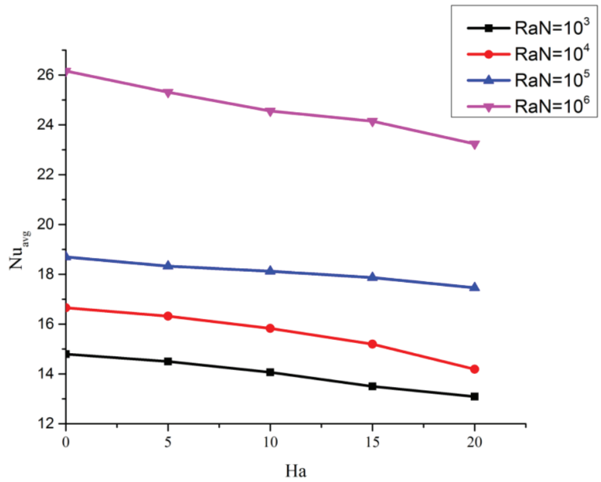

(d) $\chi = 6\%$

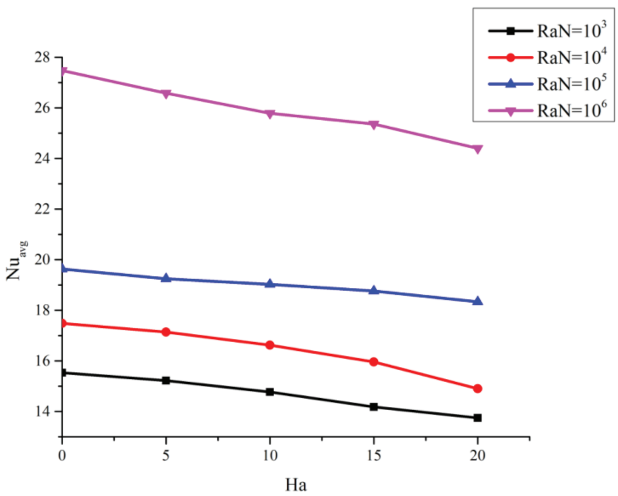

(e) $\chi = 8\%$

Figure 7. Impact of Ha on the Nu_{avg}.

CONCLUSION

This numerical study investigates the impact of buoyancy forces, magnetic field strength, and nanoparticles on fluid flow and heat transfer within a enclosure. The results show that increasing the RaN from 10^3 to 10^6 leads to intense fluid circulations, resulting in increased heat transfer. Additionally, incorporating Ag nanoparticles into the base fluid significantly improves heat transfer, with nanoparticle volume fractions rising from 2% to 8% resulting in a 25% enhancement in Nu_{avg}. However, the application of a magnetic strength, with Ha increasing from 0 to 20, causes a notable declination in heat transfer caused by the suppression of convective currents by the Lorentz force, leading to a 40% decrease in Nu_{avg} at Ha = 20. This study's findings have broad applications in industries requiring precise thermal management especially relating to the thermal energy storage and conversion systems.

NOMENCLATURE

Ag	Silver
B_o	Magnetic field flux
C_p	Specific heat capacity, (J/ Kg K)
g	Standard acceleration due to gravity, (m/s^2)
Ha	Hartmann number
k	Thermal conductivity of fluids , (W /m K)
NF	Nanofluid
RaN	Rayleigh number
$\bar{T}$	dimensional temperature, (K)
$\bar{u}$, $\bar{v}$	dimensional x and y components of velocity, (ms^{-1})
$\bar{U}$, $\bar{V}$	dimensionless velocities
x, y	dimensional coordinates, (m)

Greek symbols

α	thermal diffusivity,(m^2s^{-1})
χ	nanoparticles volume fraction
$\bar{\theta}$	non dimensional temperature
ρ	Density, (kg m^{-3})
σ	Electrical conductivity, (μS cm^{-1})

Subscripts

c	cold surface
f	fluid
n_f	nanofluid
s	Solid particles

DATA AVAILABILITY STATEMENT

The authors confirm that the data that supports the findings of this study are available within the article. Raw data that support the finding of this study are available from the corresponding author, upon reasonable request.

CONFLICT OF INTEREST

The author declared no potential conflicts of interest with respect to the research, authorship, and/or publication of this article.

ETHICS

There are no ethical issues with the publication of this manuscript.

STATEMENT ON THE USE OF ARTIFICIAL INTELLIGENCE

Artificial intelligence was not used in the preparation of the article.

REFERENCES

[1] Ostrach S. Natural convection in enclosures. ASME J Heat Transf 1988;110:1175−1190. [CrossRef]
[2] Choi SU, Eastman JA. Enhancing thermal conductivity of fluids with nanoparticles. Lemont: Argonne National Laboratory; 1995. [CrossRef]
[3] Mishra S, Pati AK, Misra A, Mishra SK. Thermal performance of nanofluid flow along an isothermal vertical plate with velocity, thermal, and concentration slip boundary conditions employing Buongiorno's revised non-homogeneous model. East Eur J Phys 2024;8:98−106. [CrossRef]
[4] Pati AK, Mishra S, Misra A, Mishra SK. Heat and mass transport aspects of nanofluid flow towards a vertical flat surface influenced by electrified nanoparticles and electric Reynolds number. East Eur J Phys 2024;1:234−241. [CrossRef]
[5] Pati AK, Misra A, Mishra SK, Mishra S, Sahu R, Panda S. Computational modelling of heat and mass transfer optimization in copper water nanofluid flow with nanoparticle ionization. JP J Heat Mass Transf 2023;31:1−8. [CrossRef]
[6] Sharma R, Aruna D, Mishra MK, Sinha SB. Scrutiny of flow and heat transfer characteristics of hybrid nanofluid passing through a squeezing channel. Sigma J Eng Nat Sci 2024;42:1856−1865. [CrossRef]
[7] Akbari N, Gholinia M, Gholinia S, Dabbaghian S, Ganji DD. Analytical and numerical study of hydrodynamic nano fluid flow in a two-dimensional semi-porous channel with transverse magnetic field. Sigma J Eng Nat Sci 2018;36:587−608.
[8] Gholinia M, Javadi H, Gatabi A, Khodabakhshi A, Ganji DD. Analytical study of a two-phase revolving system of nanofluid flow in the presence of a magnetic field to improve heat transfer. Sigma J Eng Nat Sci 2019;37:340−360.
[9] Oreper GM, Szekely J. The effect of an externally imposed magnetic field on buoyancy driven flow in a rectangular cavity. J Cryst Growth 1983;64:505−515. [CrossRef]
[10] Ozoe H, Maruo E. Magnetic and gravitational natural convection of melted silicon-two-dimensional numerical computations for the rate of heat transfer: Heat transfer, combustion, power, thermo-physical properties. JSME Int J 1987;30:774−784. [CrossRef]

[11] Rudraiah N, Barron RM, Venkatachalappa M, Subbaraya CK. Effect of a magnetic field on free convection in a rectangular enclosure. Int J Eng Sci 1995;33:1075–1084. [CrossRef]
[12] Saha T, Islam T, Yeasmin S, Parveen N. Thermal influence of heated fin on MHD natural convection flow of nanofluids inside a wavy square cavity. Int J Thermofluids 2023;18:100338. [CrossRef]
[13] Rahman MM, Chamkha AJ, Elmasry Y, Ullah I, Pasha AA, Sadeghi MS, et al. The heat transfer behavior of MHD micro-polar MWCNT-Fe3O4/water hybrid nano-fluid in an inclined shaped cavity with semi-circular heat source inside. Case Stud Therm Eng 2022;38:102316. [CrossRef]
[14] Javed T, Siddiqui MA. Effect of MHD on heat transfer through ferrofluid inside a square cavity containing obstacle/heat source. Int J Therm Sci 2018;125:419–427. [CrossRef]
[15] Balla CS, Kishan N, Gorla RS, Gireesha BJ. MHD boundary layer flow and heat transfer in an inclined porous square cavity filled with nanofluids. Ain Shams Eng J 2017;8:237–254. [CrossRef]
[16] Selimefendigil F, Oztop HF. Mixed convection of nanofluids in a three dimensional cavity with two adiabatic inner rotating cylinders. Int J Heat Mass Transf 2018;117:331–343. [CrossRef]
[17] Sheikholeslami M, Gorji-Bandpy M, Ganji DD, Soleimani S. Natural convection heat transfer in a cavity with sinusoidal wall filled with CuO-water nanofluid in presence of magnetic field. J Taiwan Inst Chem Eng 2014;45:40–49. [CrossRef]
[18] Rahman MM, Alam MS, Al-Salti N, Eltayeb IA. Hydromagnetic natural convective heat transfer flow in an isosceles triangular cavity filled with nanofluid using two-component nonhomogeneous model. Int J Therm Sci 2016;107:272–288. [CrossRef]
[19] Sreedevi P, Reddy PS. Effect of magnetic field and thermal radiation on natural convection in a square cavity filled with TiO2 nanoparticles using Tiwari-Das nanofluid model. Alex Eng J 2022;61:1529–1541. [CrossRef]
[20] Acharya N, Chamkha AJ. On the magnetohydrodynamic Al2O3-water nanofluid flow through parallel fins enclosed inside a partially heated hexagonal cavity. Int Commun Heat Mass Transf 2022;132:105885. [CrossRef]
[21] Uddin MJ, Al-Balushi J, Mahatabuddin S, Rahman MM. Convective heat transport for copper oxide-water nanofluid in an isosceles triangular cavity with a rippled base wall in the presence of magnetic field. Int J Thermofluids 2022;16:100195. [CrossRef]
[22] Dutta S, Goswami N, Biswas AK, Pati S. Numerical investigation of magneto hydrodynamic natural convection heat transfer and entropy generation in a rhombic enclosure filled with Cu-water nanofluid. Int J Heat Mass Transf 2019;136:777–798. [CrossRef]
[23] Alhajaj Z, Bayomy AM, Saghir MZ. A comparative study on best configuration for heat enhancement using nanofluid. Int J Thermofluids 2020;7:100041. [CrossRef]
[24] Fayz-Al-Asad M, Munshi MJ, Bhowmik RK, Sarker MM. MHD free convection heat transfer having vertical fin in a square wavy cavity. Int J Stat Appl Math 2019;4:32–38.
[25] Alqaed S, Mustafa J, Sharifpur M. Numerical investigation and optimization of natural convection and entropy generation of alumina/H2O nanofluid in a rectangular cavity in the presence of a magneticfield with artificial neural networks. Eng Anal Bound Elements 2022;140:507–518. [CrossRef]
[26] Song ZJ, Khan ZH, Ahmad R, Khan WA, Wei Y. Thermal analysis of ferromagnetic nanofluid flow in a channel over a dimpled cavity. J Magn Magn Mater 2023;573:170653. [CrossRef]
[27] Sunil Kumar K, Muniamuthu S, Salunkhe S, Čep R, Abouel Nasr E. In-situ analysis on drop in thermal performance of wind turbine gearbox system: Global challenges and sustainable ideas. Eng Res Express 2025;7:015243. [CrossRef]
[28] Bishnoi D. Pressure exertion and heat dissipation analysis on uncoated and ceramic (Al2O3, TiO2 and ZrO2) coated braking pads. Mater Today Proceed 2023;74:774–787. [CrossRef]
[29] Kumar SK, Muniamuthu S, Mohan A, Amirthalingam P, Anbu Muthuraja M. Effect of charging and discharging process of PCM with paraffin and Al2O3 additive subjected to three point temperature locations. J Ecol Eng 2022;23:34–42. [CrossRef]
[30] Kumar KS, Raju DB, Arulmani J, Amirthalingam P. Design and structural analysis of liquified cryogenic tank under seismic and operating loading. Int J Mech Eng Technol 2016;7:345–366.
[31] Godson L, Deepak K, Enoch C, Jefferson B, Raja B. Heat transfer characteristics of silver/water nanofluids in a shell and tube heat exchanger. Arch Civil Mech Eng 2014;14:489–496. [CrossRef]
[32] Selvam C, Irshad EM, Lal DM, Harish S. Convective heat transfer characteristics of water-ethylene glycol mixture with silver nanoparticles. Exper Therm Fluid Sci 2016;77:188–196. [CrossRef]
[33] Pourhoseini SH, Naghizadeh N, Hoseinzadeh H. Effect of silver-water nanofluid on heat transfer performance of a plate heat exchanger: An experimental and theoretical study. Powder Technol 2018;332:279–286. [CrossRef]
[34] Wang D, Dhahad HA, Ali MA, Almojil SF, Almohana AI, Alali AF, et al. A comparative numerical analysis and environment assessment to examine hydrothermal behavior of two serpentine heatsink with water/silver Nano fluid applying two-phase mixture model. Eng Anal Bound Elements 2023;146:966–976. [CrossRef]

[35] Shahsavar A, Baseri MM, Al-Rashed AA, Afrand M. Numerical investigation of forced convection heat transfer and flow irreversibility in a novel heatsink with helical microchannels working with biologically synthesized water-silver nano-fluid. Int Commun Heat Mass Transf 2019;108:104324. [CrossRef]
[36] Al-Rashed AA, Shahsavar A, Rasooli O, Moghimi MA, Karimipour A, Tran MD. Numerical assessment into the hydrothermal and entropy generation characteristics of biological water-silver nano-fluid in a wavy walled microchannel heat sink. Int Commun Heat Mass Transf 2019;104:118–126. [CrossRef]
[37] Rashmi MR, Kola R, Kumar M, Pratyush K, Dule P, Sivasankar GA. Investigation of heat transfer for silver oxide (Ag2O) and iron oxide (Fe3O4) using nano fluid over a stretch sheet. Mater Today Proceed 2022;69:1118–1125. [CrossRef]
[38] Domakonda VK, Shaik Farooq. Natural convection characteristics of copper-water nano fluid with two heat sources at the bottom surface in a square enclosure-a numerical study. Int J Heat Technol 2020;38:395–404. [CrossRef]
[39] Shaik Farooq, Domakonda VK. Numerical study on natural convection of alumina-water nanofluid in a square cavity with two localized heat sources on adjacent surfaces. Period Polytech Mech Eng 2021;65:217–228. [CrossRef]
[40] Brinkman HC. The viscosity of concentrated suspensions and solutions. J Chem Phys 1952;20:571. [CrossRef]
[41] Maxwell JC. A treatise on electricity and magnetism. Oxford: Clarendon Press; 1873.
[42] Selimefendigil F, Chamkha AJ. MHD mixed convection of Ag-MgO/water nanofluid in a triangular shape partitioned lid-driven square cavity involving a porous compound. J Therm Anal Calorim 2021;143:1467–1484. [CrossRef]
[43] Patankar SV. Numerical heat transfer and fluid flow. Washington, DC: Hemisphere Publishing Corporation; 1980.
[44] Ghasemi B, Aminossadati SM, Raisi A. Magnetic field effect on natural convection in a nanofluid-filled square enclosure. Int J Therm Sci 2011;50:1748–1756. [CrossRef]
[45] Islam T, Alam MN, Asjad MI, Parveen N, Chu YM. Heatline visualization of MHD natural convection heat transfer of nanofluid in a prismatic enclosure. Sci Rep 2021;11:10972. [CrossRef]
[46] Mirzaei A, Jalili B, Jalili P, Ganji DD. Free convection in a square wavy porous cavity with partly magnetic field: A numerical investigation. Sci Rep 2024;14:14152. [CrossRef]
[47] Bakar NA, Karimipour A, Roslan R. Effect of magnetic field on mixed convection heat transfer in a lid-driven square cavity. J Thermodyn 2016;2016:3487182. [CrossRef]